Title

Protease-Responsive Potential-Tunable AIEgens for Cell Selective Imaging of TMPRSS2 and Accurate Inhibitor Screening.

Journal

Analytical Chemistry, 95(7)

Authors

Cheng, Yong

Clark, Alex

Yim, Wonjun

et al.

Publication Date

2023-02-21

DOI

10.1021/acs.analchem.2c04988

Peer reviewed

HHS Public Access

Author manuscript

Anal Chem. Author manuscript; available in PMC 2024 February 21.

Published in final edited form as:

Anal Chem. 2023 February 21; 95(7): 3789–3798. doi:10.1021/acs.analchem.2c04988.

Protease-Responsive Potential-Tunable AIEgens for Cell Selective Imaging of TMPRSS2 and Accurate Inhibitor Screening

Yong Cheng,
Department of NanoEngineering, University of California, San Diego, La Jolla, California 92093, United States

Alex E. Clark,
Department of Medicine, University of California, San Diego, La Jolla, California 92093, United States

Wonjun Yim,
Materials Science and Engineering Program, University of California, San Diego, La Jolla, California 92093, United States

Raina M. Borum,
Department of NanoEngineering, University of California, San Diego, La Jolla, California 92093, United States

Yu-Ci Chang,
Materials Science and Engineering Program, University of California, San Diego, La Jolla, California 92093, United States

Zhicheng Jin,
Department of NanoEngineering, University of California, San Diego, La Jolla, California 92093, United States

Tengyu He,
Materials Science and Engineering Program, University of California, San Diego, La Jolla, California 92093, United States

Aaron F. Carlin,
Department of Medicine and Department of Pathology, University of California, San Diego, La Jolla, California 92093, United States

Jesse V. Jokerst
Department of NanoEngineering, Materials Science and Engineering Program, and Department of Radiology, University of California, San Diego, La Jolla, California 92093, United States

Abstract

Corresponding Author: Jesse V. Jokerst – Department of NanoEngineering, Materials Science and Engineering Program, and Department of Radiology, University of California, San Diego, La Jolla, California 92093, United States; jjokerst@ucsd.edu.

The authors declare no competing financial interest.

Complete contact information is available at: https://pubs.acs.org/10.1021/acs.analchem.2c04988

Transmembrane protease serine 2 (TMPRSS2) is a plasma membrane protease that activates both spike protein of coronaviruses for cell entry and oncogenic signaling pathways for tumor progression. TMPRSS2 inhibition can reduce cancer invasion and metastasis and partially prevent the entry of SARS-CoV-2 into host cells. Thus, there is an urgent need for both TMPRSS2-selective imaging and precise screening of TMPRSS2 inhibitors. Here, we report a TMPRSS2-responsive surface-potential-tunable peptide-conjugated probe (EGTP) with aggregation-induced emission (AIE) features for TMPRSS2 selective imaging and accurate inhibitor screening. The amphiphilic EGTP was constructed with tunable surface potential and responsive efficiency with TMPRSS2 and its inhibitor. The rational construction of AIE luminogens (AIEgens) with modular peptides indicated that the cleavage of EGTP led to a gradual aggregation with bright fluorescence in high TMPRSS2-expressing cells. This strategy may have value for selective detection of cancer cells, SARS-CoV-2-target cells, and screening of protease inhibitors.

Graphical Abstract

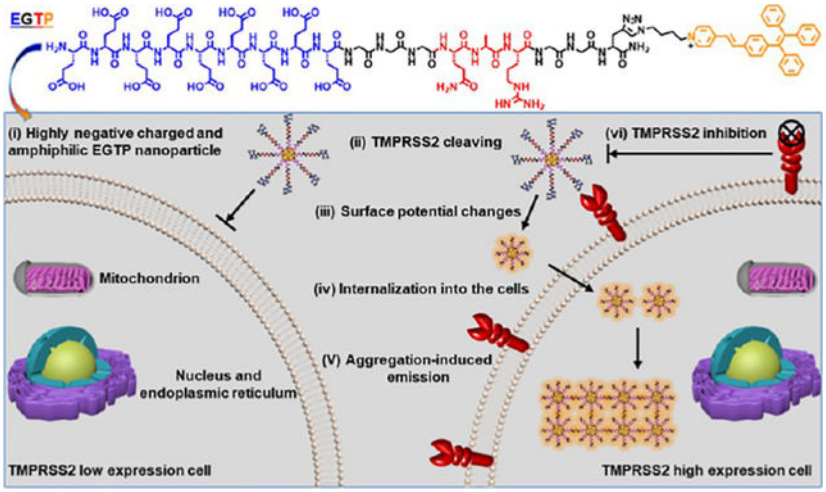

INTRODUCTION

Transmembrane protease serine 2 (TMPRSS2) is a cell membrane protease that is highly expressed in epithelial cells of the nose, lung, colon, gallbladder, kidney, and prostate, and plays key roles in tissue homeostasis.[1–3] TMPRSS2 has a transmembrane domain, a linker region, and a canonical serine protease domain with both proteolytic and signal transduction activity.[4–6] TMPRSS2 can cleave after the peptide sequence QAR.[7,8] Aberrant expression of TMPRSS2 in cancer cells suggests it may be used as a diagnostic biomarker and possibly as a therapeutic target.[9,10] Some coronaviruses and influenza viruses are also dependent on TMPRSS2 for viral activation and cell entry.[11–16] TMPRSS2 inhibitors can reduce prostate cancer cell invasion and metastasis and partially prevent the entry of SARS-CoV-2 into the lung epithelial cells.[17–20] Monitoring TMPRSS2 activity has attracted broad attention due to its important value in imaging cancer cells, viral infection, and identification of inhibitors,[21–23] which has led to the development of fluorogenic peptide substrates and immunofluorescence antibodies.[24–27] TMPRSS2 selective imaging and accurate TMPRSS2

inhibitor screening may improve the diagnosis and treatment of cancer as well as COVID-19 and other emerging viruses.

Fluorescence imaging has been widely used because of its high sensitivity, excellent resolution, multicolor labeling, and rapid signal acquisition.[28–30] There are several signal conversion mechanisms to design enzymatic fluorescent probes, like intramolecular charge transfer, photon-induced electron transfer, Förster resonance energy transfer, and aggregation-induced emission (AIE).[31–33] Among them, the fluorescence intensity of AIE luminogens (AIEgens) responds to changes in restriction of intramolecular motion with polarity or molecular-rotation-limited environment.[34,35] Propeller-shaped AIEgens have been widely applied to optical devices, luminescent sensors, imaging probes, and cancer theranostic.[36] For example, the bright yellow fluorescence, mitochondrial targeting, and superior photostability of AIEgen azide-functionalized tetraphenylethene pyridinium (PyTPE) is beneficial for real-time long-term cell imaging.[37,38] Notably, the fluorescent intensity of PyTPE can be enhanced after the cleavage of peptides, nucleic acids, and glycans with proteases.[39,40] To focus on extracellular proteases, Tsien and co-workers developed protease-activatable cell-penetrating peptide probes where the positively charged cell-penetrating peptides are initially neutralized by polyanionic sequences.[41,42] Specific protease cleavage liberates the polycationic peptide linked probe, which binds and enters cells for imaging. Creating a positively charged AIEgens peptide with a cell surface protease-removable polyanionic peptide could reduce non-specific aggregation of positive charged AIEgens inside cells and restrict probe cleavage to extracellular proteases.

Herein, we developed a protease-responsive and surface-potential-tunable peptide-conjugated AIEgens (EGTP) for TMPRSS2-selective imaging and accurate inhibitor screening (Scheme 1). EGTP consists of four segments: the first is a polyglutamic acid (Glu, **E** for short in EGTP) that increases the solubility and blocks PyTPEs' positive charges and cell-penetrating ability.[43,44] Second, the spacer trimylglycine (GGG, **G**) is designed to enhance probe flexibility and reduce steric hindrance for TMPRSS2-related substrate interactions.[45] The third component is the TMPRSS2-responsive peptide (QAR, **T**), which can be cleaved by TMPRSS2 after the QAR sequence.[7,8,25] The fourth is a positive charged AIEgens (PyTPE, **P**).[33,37,38] These four components were covalently coupled through Fmoc-based solid-phase peptide synthesis and copper-catalyzed azide–alkyne click reaction. We found that in the absence of TMPRSS2, EGTP is a highly negatively charged and amphiphilic molecule that can be highly water-soluble with limited fluorescence (Scheme 1a).[46] After cleavage by TMPRSS2, the hydrophilic polyglutamic acid segment is separated from the PyTPE segment. Decreasing hydrophilicity leads to PyTPE aggregation and strong fluorescence, which is blocked by the TMPRSS2 inhibitor. Thus, EGTP cleavage by high TMPRSS2 expressing cells releases PyTPE that crosses the cell membrane and aggregates with enhanced fluorescence (Scheme 1b). This probe will provide a controllable avenue for protease-selective imaging and accurate inhibitor screening in cell-based models.

EXPERIMENTAL SECTION

Materials, Methods, Synthesis, and Characterization of PyTPE, EGTP, TGP, and EGEP.

For further details, please see the Supporting Information.

Enzymatic Assay with EGTP, TGP, and EGEP.

The stock solution of PyTPE, EGTP, TGP, and EGEP in 20 mM Tris–HCl buffer (pH = 8.0) was diluted with TMPRSS2 assay buffer (20 mM Tris–HCl buffer (pH 8.0) with 150 mM NaCl, 1 mM DTT, and 5% glycerol) to make 1, 5, 10, and 20 μM working solutions. Recombinant TMPRSS2 was added into the working solution and then diluted to a total of 100 μL with the same Tris–HCl buffer. The reaction mixture was incubated at 37 °C for 1 h for UV–vis absorption and fluorescence measurement. The solution was excited at 405 nm, and the emission was collected from 430 to 800 nm.

Cell Culture and Plasmid Transfection.

All the cells were cultured in Dulbecco's modified Eagle medium (DMEM) with 10% fetal calf serum (FBS) and 1% penicillin streptomycin (PS, 10,000 IU penicillin and 1000 μg/mL streptomycin, multicell) in cell culture plates at 37 °C in a humidified atmosphere containing 5% CO_2.

Incubation of Cells with Probes.

For confocal laser scanning microscopy (CLSM) imaging, A549 cells, HeLa cells, MCF-7-GFP cells, Vero cells, and TMPRSS2-Vero cells were seeded into cell culture dishes at a density of 2.0×10^5 in growth medium (DMEM supplemented with 10% FBS, 200 mL). After overnight incubation, the cells were washed with phosphate-buffered saline (PBS, pH 7.4) three times. A solution of the indicated probe in PBS was then added, and the cells were incubated in a 5% CO_2 atmosphere at 37 °C for further use. Hoechst 33258 and MTG (or Alexa Fluor 488 or Alexa Fluor 647) were subsequently added for probe incubation. The supernatant was then discarded, and the cells were washed gently twice with PBS and fixed with 2% paraformaldehyde at room temperature for 20 min prior to optical imaging.

Immunofluorescence.

Fixed cells were washed with PBS and then with PBS including 1% BSA and 0.1% Triton X-100. Cells were incubated with primary antibody against TMPRSS2 (1:100, abcam and Thermo Fisher Scientific) in PBS including 1% BSA and 0.1% Triton X-100 overnight at 4 °C. Cells were washed and incubated with Alexa 488 or Alexa 647 goat anti-rabbit secondary antibody (abcam and Thermo Fisher Scientific) in PBS including 1% BSA for 1 h at room temperature followed by 3× PBS washes.

Confocal Laser Scanning Microscopy.

The fluorescence signals of cells were detected using a Zeiss LSM 880 CLSM (Zeiss), equipped with a 63/1.42 numerical aperture oil-immersion objective lens. A 405 nm laser was chosen for the excitation of Hoechst 33258, and the emission was collected at 420–460 nm. A 405 nm laser was chosen for the excitation of AIEgens, and the emission was collected at 550–620 nm. A 488 nm laser was chosen for the excitation of GFP (or MTG, or Alexa 488), and the emission was collected at 500–530 nm. A 633 nm laser was chosen for the excitation of Alexa 647, and the emission was collected at 650–720 nm. All fluorescence images were analyzed with Zeiss Image software (Zeiss).

Cytotoxicity Assay.

The cytotoxic potential of PyTPE, EGT, EGTP, TGP, and EGEP were assessed using the A549 cells, HeLa cells, and MCF-7 cells for 48 h incubation in quadruplicate in a 96-well plate. The fluorescence of Resazurin solution at 690 nm using an excitation wavelength of 560 nm was recorded by a Synergy H1 microplate reader (BioTek) with standard operation procedures.

RESULTS AND DISCUSSION

Design, Synthesis, and Characterization of EGTP and Its Derivatives.

EGTP was designed to be activatable and cell-penetrating based on the AIE effect after a TMPRSS2 trigger (Figure 1a). EGTP mainly involves a peptide part (EGT) and AIEgen part (PyTPE). The polyglutamic acid (EEEEEEEEE) was placed at the N-terminal. Importantly, the QAR sequence is a substrate for TMPRSS2 cleavage: Cleavage of QAR changes the hydrophobicity and hydrophilicity of the system and facilitates cell uptake. Trimylglycine (GGG) linkers were added at both ends of the TMPRSS2 substrate to leave space for enzyme and substrate binding. Propargylglycine (Pra) is used as a linker at the N-terminal to react with PyTPE. All domains are coupled via Fmoc-based solid-phase peptide synthesis and a copper-catalyzed click reaction. After TMPRSS2 cleavage, EGTP is divided into the hydrophilic EEEEEEEEEGGGQAR and the hydrophobic GG(Pra)-PyTPE. Two control probes that lacked the polyglutamic acid sequence (TGP) or the TMPRSS2-responsive peptide (EGEP) are synthesized to verify TMPRSS2-mediated activation. All probes are synthesized according to previous reports (Schemes S1–S4).[32,33,37,38] The molecules were characterized by high performance liquid chromatography (HPLC, Figures 1b and S1), electrospray ionization mass spectrometry (ESI-MS, Figures 1c–e and S2,S4 and S7), and high-resolution mass spectra (Figures S3,S5, and S8) to confirm their purity (at least 95%) and chemical structures. Taking EGTP, for example, Figure 1d shows a strong peak at 1225.12 attributed to the $[M + 2H]^{2+}$ ion of EGTP (calcd, 1224.51286) as well as a strong peak at 816.90 attributed to the $[M + 3H]^{3+}$ ion of EGTP (calcd, 816.6815). The mass data of TGP and EGEP also matched well with the calculated data. These data indicated that EGTP, TGP, and EGEP were synthesized successfully.

Responsiveness to Enzyme in Solutions.

We first evaluated whether the probes can be specifically cleaved by recombinant TMPRSS2 as predicted. HPLC and ESI-MS analysis confirmed that EGTP and TGP but not EGEP can be cleaved by TMPRSS2 between R and G after incubation for 1 h at 37 °C in 20 mM Tris–HCl buffer (pH 8.0) (Figures 1b,e and S6 and S9). Dynamic light scattering (DLS) tests and transmission electron microscopy (TEM) of EGTP, TGP, and EGEP were performed to determine the change of particle size, surface potential distribution, and particle morphology after incubation with TMPRSS2 (Figures S10 and S11). For 20 μM EGTP, the average hydrodynamic size increased from 79 to 352 nm (Figure 1f), and the mean zeta potential value increased from −23.8 to −16.6 mV (Figures 1g and S12), suggesting nanoparticle aggregation and a reduction of polyglutamic acid on the particle surface. Their morphology changes with TMPRSS2 incubation were confirmed by TEM (Figures 1h and S13). These

data proved that EGTP and TGP but not EGEP is responsive to TMPRSS2 leading to an aggregated state and surface potential changes.

We then explored the spectral properties of PyTPE, EGTP, TGP, and EGEP. They had absorption spectral profiles at 320–490 nm in Tris–HCl buffer with 1% DMSO (Figures 2a and S14); 405 nm was thus chosen as the optimal excitation wavelength. The fluorescence spectral profiles of PyTPE, EGTP, TGP, and EGEP were 500–750 nm. Their fluorescence intensities decreased after being modified with hydrophilic peptides, and the wavelength is redshifted (Figure 2b). Particularly, the fluorescence intensity of TGP was stronger than that of EGTP and EGEP because of the lack of the hydrophilic polyglutamic acid.[46] The fluorescence changes of EGTP were monitored upon incubation with TMPRSS2: 20 μM offered significant fluorescence enhancement and was used for subsequent experiments (Figure S15).

To further validate the enzyme digestion efficiency, different concentrations of EGTP were incubated with different concentrations of TMPRSS2 (Figures 2c,d and S16). The fluorescence intensity of EGTP increased 22.61-fold and 9.96-fold with increasing concentrations of both EGTP and TMPRSS2. But EGTP did not reach the equivalent fluorescence intensity of PyTPE at the same concentration, likely because hydrophilic residues (G and Pra) remain linked with PyTPE after cleavage (Figure S17). Subsequent kinetic studies were performed by incubating EGTP with TMPRSS2 and camostat mesylate (i.e., camostat), a TMPRSS2 serine protease inhibitor (Figure 2e).[20,27] The fluorescence intensity of EGTP at 590 nm increased over time in the presence of TMPRSS2 and was blocked by camostat.

EGTP was treated under identical conditions with several commercial mammalian and viral proteases, proteins, and different media to investigate probe specificity and stability (Figures 2f and S18). The fluorescence intensity of EGTP selectively increased 4.7-fold higher in the presence of TMPRSS2. Trypsin caused some fluorescence enhancement (2.3-fold) due to its cleavage after arginine (R) in the peptide sequence.[47] Our results showed the tryptic digestion of EGTP has less cleavage efficiency than TMPRSS2. Trypsin has limited impact on TMPRSS2 detection, and its interference can be controlled and minimized via probe concentrations and incubation time. Camostat reduced TMPRSS2-dependent EGTP fluorescence to a greater degree than incubation with GC376, a cysteine protease inhibitor, or GRL0617, a papain-like cysteine protease inhibitor, that have activity against SARS-CoV-2 main protease (M^{pro}) and papain-like protease (PL^{pro}), respectively (Figure 2g).[32] The inhibition of fluorescence intensity was linearly correlated with camostat concentration (Figure 2h). These results demonstrate that EGTP can detect recombinant TMPRSS2 and TMPRSS2 inhibitors in buffer or cell culture medium.

TMPRSS2 Selective Imaging in Cancer Cells with EGTP.

The TMPRSS2 selective imaging of EGTP was tested via three different cell lines. A549 cells and HeLa cells express TMPRSS2 at low levels, while MCF-7-GFP cells (with a GFP reporter gene for stable expression of GFP in order to distinguish from other cell lines) express TMPRSS2 at high levels as confirmed by flow cytometry with Alexa Fluor 647-labeled antibody (Alexa 647) (Figure S19).[3,21,48,49] These cell lines were cultured alone

or co-cultured in the presence of PyTPE, EGTP, TGP, EGTP, Hoechst 33258 (nucleus staining), Mito tracker green (MTG), TMPRSS2 primary antibody, and Alexa Fluor 647-labeled secondary antibody (Alexa 647) for CLSM observation (Figure 3a). We observed that the yellow fluorescence of PyTPE overlapped well with the green fluorescence of MTG in the HeLa cells due to the hydrophobic effect and electrostatic interactions of positively charged pyridinium unit and hydrophobic alkyl chain to confirm that PyTPE is suitable for cell imaging (Figure 3b).[38] We then used immunofluorescence imaging to validate the TMPRSS2 relative expression among these three cell lines with Alexa 647 (Figures 3c and S20). The relative fluorescence intensity of A549 cells, HeLa cells, and MCF-7-GFP cells was 0.68, 0.95, and 16.99, which was similar to the RNA expression reported data (the resulting normalized transcript expression values (*n*TPM) calculated for each gene in every sample are 0, 0.1, and 10.5 for A549, HeLa, and MCF-7-GFP, respectively).[49]

In addition, to examine the cytotoxicity and optimize the concentration of each probe for cell imaging, different concentrations, between 1 and 20 μM, of PyTPE, EGT, EGTP, TGP, and EGEP were incubated with A549 cells, HeLa cells, and MCF-7-GFP cells for 48 h under standard cell culture conditions (Figure S21). EGT and EGEP showed negligible toxicity to these cells with almost 100% cell viability at the tested concentrations. High concentrations of PyTPE (>5 μM), EGTP (>10 μM), and TGP (>10 μM) can cause significant cytotoxicity. CLSM images of MCF-7-GFP cells showed a good signal to noise ratio and stronger yellow fluorescence of EGTP at higher concentrations (10 μM) versus the fluorescence of 5 μM EGTP incubation (Figure S22). Therefore, 10 μM EGTP was used for cell imaging experiments.

Under the same staining condition, A549 cells showed almost no yellow fluorescence (Figure 3d). There is no TMPRSS2 expression, no cleavage of EGTP, and no GG(Par) PyTPE signal in the A549 cells. Only weak yellow fluorescence was displayed in the HeLa cells (Figure 3e). Strong green and yellow fluorescence were both observed in the MCF-7-GFP cells (Figure 3f). We also found that the yellow (EGTP) and red (Alexa 647) fluorescence signals relate to TMPRSS2 expression levels and are different across a population of MCF-7-GFP cells (Figures S23 and S24). Importantly, co-cultured MCF-7-GFP and A549 cells (MCF-7-GFP and A549 cells) showed that only MCF-7-GFP cells (white dotted ring) have strong green and yellow fluorescence signals, thus indicating that TMPRSS2 can uniquely identify TMPRSS2 expressing cells (Figure 3g–i). Importantly, A549 cells showed little yellow fluorescence in the MCF-7-GFP and A549 co-cultured cells due to the nonspecific internalization of GG(Pra)-PyTPE after the cleavage of EGTP by TMPRSS2 from MCF-7-GFP cells (Figure S24c). Strong yellow fluorescence signals of EGTP were observed in the co-cultured A549 cells with the increasing incubation time (Figure S25). In contrast, A549 cells, HeLa cells, and MCF-7-GFP cells all showed strong yellow fluorescence during TGP incubation due to the lack of polyglutamic acid and nonspecific internalization by positive charged units (Figures S26 and S27). Additionally, there was minimal yellow fluorescence observed in MCF-7-GFP cultured with and without A549 cells during EGEP incubation, which lacks the QAR protease cleavage sequence required to release the polyglutamic acid segment (Figure S28). We had to control the incubation time of probes with cells to avoid these false positive signals caused the aggregation of probes by the positively charged proteins or the nonspecific cleavage by

other proteases outside the cytomembrane (Figure S29). These data verify that EGTP detects the TMPRSS2 expression in individual cells through proteolytic release of the polyglutamic acid segment.

TMPRSS2 Selective Imaging and Inhibition of Vero Cells and TMPRSS2-Vero Cells with EGTP and Camostat.

We next validated the ability of EGTP to screen for TMPRSS2 inhibitors using Vero E6 cells with (TMPRSS2-Vero) and without (Vero) the TMPRSS2 expression (Figure 4a). Vero cells and TMPRSS2-Vero cells (Recombinant clonal stable Vero E6 cell line constitutively expressing full length human TMPRSS2) were incubated with different concentrations (1, 5, 10, and 20 μM) of PyTPE and EGTP (Figures S30–S33). The expression of TMPRSS2 in Vero and TMPRSS2-Vero cells was confirmed by TMPRSS2 primary antibodies with Alexa Fluor 488 (Alexa 488) labeled secondary antibodies (Figure 4b,c). The yellow fluorescence of PyTPE observed and enhanced with increasing concentrations both in the Vero cells and TMPRSS2-Vero cells, while the yellow fluorescence of EGTP was selectively observed in TMPRSS2-Vero cells (Figure 4d,e). The yellow fluorescence of EGTP and green fluorescence of Alexa 488 showed that the TMPRSS2 distribution is different for each cell (Figure S34).

After validating that EGTP activation was TMPRSS2-dependent in TMPRSS2-Vero cells, we then tested whether EGTP could measure TMPRSS2 inhibition in a cell-based model (Figure 5a). TMPRSS2-Vero cells were incubated with different concentrations (0, 1, 10, 100, and 1000 μM) of camostat before adding EGTP and Hoechst 33258 (Figure 5b–f). EGTP yellow fluorescence decreased with increasing concentrations of camostat (Figure S35), but the yellow fluorescence did not change in the presence of GC376 or GRL0617 (Figure S36). These data confirm that EGTP can identify TMPRSS2 inhibitors in living cells.

CONCLUSIONS

In summary, this work demonstrated a TMPRSS2-responsive and surface-potential-tunable peptide-conjugated probe (EGTP) with multifunctional peptides and AIEgen for selective imaging of TMPRSS2 in MCF-7-GFP and TMPRSS2-Vero cells. We utilized the positive charged PyTPE for cell internalization and imaging, the negative charged polyglutamic acid to block internalization, and the TMPRSS2-responsive sequence to regulate the internalization and aggregation of PyTPE. Importantly, the delivery process and AIE effect of EGTP were controlled by the rational composition of the modular-peptides. In contrast to control probes without negatively charged polyglutamic acid (TGP) or the TMPRSS2-responsive sequence (EGEP), EGTP is both effectively cleaved by TMPRSS2 and forms aggregates with bright yellow fluorescence. We verified that EGTP accurately identifies TMPRSS2 expressing cells using three different cancer cell lines, Vero cells, and TMPRSS2-Vero cells. Additionally, using camostat, we show that EGTP can identify inhibitors of TMPRSS2 in a cell-based model. Future work will evaluate the probe stability and sensitivity in complex environments for studies of cell migration, cell–cell interactions, cell tracking, and clinical sample analysis. This strategy for protease-responsive

and surface-potential-tunable peptide-conjugated probes could lead to effective membrane protein imaging and accurate inhibitor screening for precise diagnosis and treatment of cancer, SARS-CoV-2, and other emerging viral infections.

Supplementary Material

Refer to Web version on PubMed Central for supplementary material.

ACKNOWLEDGMENTS

We acknowledge funding from the National Institutes of Health (R01 DE031114, R21 AI157957, and R21 AG065776–01S1) for financial support. This work was supported in part by the National Science Foundation Graduate Research Fellowship Program under grant no. DGE-1650112. This research was supported by NIH grant (K08 AI130381) and Career Award for Medical Scientists from the Burroughs Wellcome Fund to AFC. R.M.B. acknowledges fellowship support under T32 CA153915.

REFERENCES

(1). Vaarala MH; Porvari KS; Kellokumpu S; Kyllönen AP; Vihko PT J. Pathol. 2001, 193, 134–140. [PubMed: 11169526]

(2). Sungnak W; Huang N; Bécavin C; Berg M; Queen R; Litvinukova M; Talavera-López C; Maatz H; Reichart D; Sampaziotis F; Worlock KB; Yoshida M; Barnes JL; HCA Lung Biological Network. Nat. Med. 2020, 26, 681–687. [PubMed: 32327758]

(3). Lukassen S; Chua RL; Trefzer T; Kahn NC; Schneider MA; Muley T; Winter H; Meister M; Veith C; Boots AW; Hennig BP; Kreuter M; Conrad C; Eils R EMBO J. 2020, 39, No. e105114. [PubMed: 32246845]

(4). Epstein RJ Tumour. Biol. 2021, 43, 159–176. [PubMed: 34420994]

(5). Lam DK; Dang D; Flynn AN; Hardt M; Schmidt BL Pain 2015, 156, 923–930. [PubMed: 25734995]

(6). Abbasi AZ; Kiyani DA; Hamid SM; Saalim M; Fahim A; Jalal NJ Med. Virol. 2021, 93, 4205–4218.

(7). Hu X; Shrimp JH; Guo H; Xu M; Chen CZ; Zhu W; Zakharov AV; Jain S; Shinn P; Simeonov A; Hall MD; Shen M ACS Pharmacol. Transl. Sci. 2021, 4, 1124–1135. [PubMed: 34136758]

(8). Fraser BJ; Beldar S; Seitova A; Hutchinson A; Mannar D; Li Y; Kwon D; Tan R; Wilson RP; Leopold K; Subramaniam S; Halabelian L; Arrowsmith CH; Bénard F Nat. Chem. Biol. 2022, 18, 963–971. [PubMed: 35676539]

(9). Tanabe LM; List K FEBS J. 2017, 284, 1421–1436. [PubMed: 27870503]

(10). Tarnow C; Engels G; Arendt A; Schwalm F; Sediri H; Preuss A; Nelson PS; Garten W; Klenk HD; Gabriel G; Böttcher-Friebertshäuser EJ Virol. 2014, 88, 4744–4751.

(11). Esumi M; Ishibashi M; Yamaguchi H; Nakajima S; Tai Y; Kikuta S; Sugitani M; Takayama T; Tahara M; Takeda M; Wakita T Hepatology 2015, 61, 437–446. [PubMed: 25203900]

(12). Iwata-Yoshikawa N; Okamura T; Shimizu Y; Hasegawa H; Takeda M; Nagata M; Nagata NJ Virol. 2019, 93, e01815–e01818.

(13). Hoffmann M; Kleine-Weber H; Schroeder S; Krüger N; Herrler T; Erichsen S; Schiergens TS; Herrler G; Wu NH; Nitsche A; Müller MA; Drosten C; Pöhlmann S Cell 2020, 181, 271–280. [PubMed: 32142651]

(14). Shang J; Wan Y; Luo C; Ye G; Geng Q; Auerbach A; Li F Proc. Natl. Acad. Sci. U.S.A. 2020, 117, 11727–11734. [PubMed: 32376634]

(15). Zang R; Gomez Castro MFG; McCune BT; Zeng Q; Rothlauf PW; Sonnek NM; Liu Z; Brulois KF; Wang X; Greenberg HB; Diamond MS; Ciorba MA; Whelan SPJ; Ding S Sci. Immunol. 2020, 5, No. eabc3582. [PubMed: 32404436]

(16). Padmanabhan P; Desikan R; Dixit NM PLoS Comput. Biol. 2020, 16, No. e1008461. [PubMed: 33290397]

(17). Mollica V; Rizzo A; Massari F Future Oncol. 2020, 16, 2029–2033. [PubMed: 32658591]

(18). Cannalire R; Stefanelli I; Cerchia C; Beccari AR; Pelliccia S; Summa V Int. J. Mol. Sci. 2020, 21, 5707. [PubMed: 32784899]

(19). Strope JD; PharmD DC; Figg WD J. Clin. Pharmacol. 2020, 60, 801–807. [PubMed: 32437018]

(20). Hempel T; Raich L; Olsson S; Azouz NP; Klingler AM; Hoffmann M; Pöhlmann S; Rothenberg ME; Noé F Chem. Sci. 2021, 12, 983–992. [PubMed: 35382133]

(21). Zhang F; Li W; Feng J; Ramos da Silva S; Ju E; Zhang H; Chang Y; Moore PS; Guo H; Gao SJ J. Med. Virol. 2021, 93, 6671–6685. [PubMed: 34324210]

(22). Koch J; Uckeley ZM; Doldan P; Stanifer M; Boulant S; Lozach PY EMBO J. 2021, 40, No. e107821. [PubMed: 34159616]

(23). Sun YJ; Velez G; Parsons DE; Li K; Ortiz ME; Sharma S; McCray PB Jr.; Bassuk AG; Mahajan VBJ Clin. Invest. 2021, 131, No. e147973.

(24). Lu Q; Nunez E; Lin C; Christensen K; Downs T; Carson DA; Wang-Rodriguez J; Liu YT Nucleic Acids Res. 2008, 36, No. e130. [PubMed: 18794177]

(25). Shrimp JH; Kales SC; Sanderson PE; Simeonov A; Shen M; Hall MD ACS Pharmacol. Transl. Sci. 2020, 3, 997–1007. [PubMed: 33062952]

(26). Chen Y; Lear TB; Evankovich JW; Larsen MB; Lin B; Alfaras I; Kennerdell JR; Salminen L; Camarco DP; Lockwood KC; Tuncer F; Liu J; Myerburg MM; McDyer JF; Liu Y; Finkel T; Chen BB Nat. Commun. 2021, 12, 3907. [PubMed: 34162861]

(27). Shapira T; Monreal IA; Dion SP; Buchholz DW; Imbiakha B; Olmstead AD; Jager M; Désilets A; Gao G; Martins M; Vandal T; Thompson CAH; Chin A; Rees WD; Steiner T; Nabi IR; Marsault E; Sahler J; Diel DG; Van de Walle GR; August A; Whittaker GR; Boudreault PL; Leduc R; Aguilar HC; Jean F Nature 2022, 605, 340–348. [PubMed: 35344983]

(28). Guo Y; Li D; Zhang S; Yang Y; Liu JJ; Wang X; Liu C; Milkie DE; Moore RP; Tulu US; Kiehart DP; Hu J; Lippincott-Schwartz J; Betzig E; Li D Cell 2018, 175, 1430–1442. [PubMed: 30454650]

(29). Nguyen SS; Prescher JA Nat. Rev. Chem. 2020, 4, 476–489. [PubMed: 34291176]

(30). Yin J; Huang L; Wu L; Li J; James TD; Lin W Chem. Soc. Rev. 2021, 50, 12098–12150. [PubMed: 34550134]

(31). Liu HW; Chen L; Xu C; Li Z; Zhang H; Zhang XB; Tan W Chem. Soc. Rev. 2018, 47, 7140–7180. [PubMed: 30140837]

(32). Cheng Y; Borum RM; Clark AE; Jin Z; Moore C; Fajtová P; O'Donoghue AJ; Carlin AF; Jokerst JV Angew. Chem., Int. Ed. Engl. 2022, 61, No. e202113617. [PubMed: 34889013]

(33). Cheng Y; Huang F; Min X; Gao P; Zhang T; Li X; Liu B; Hong Y; Lou X; Xia F Anal. Chem. 2016, 88, 8913–8919. [PubMed: 27503607]

(34). Zhang H; Zhao Z; Turley AT; Wang L; McGonigal PR; Tu Y; Li Y; Wang Z; Kwok RTK; Lam JWY; Tang BZ Adv. Mater. 2020, 32, No. e2001457. [PubMed: 32734656]

(35). Feng G; Liu B Acc. Chem. Res. 2018, 51, 1404–1414. [PubMed: 29733571]

(36). Mei J; Leung NL; Kwok RT; Lam JW; Tang BZ Chem. Rev. 2015, 115, 11718–11940. [PubMed: 26492387]

(37). Cheng Y; Sun C; Liu R; Yang J; Dai J; Zhai T; Lou X; Xia F Angew. Chem., Int. Ed. Engl. 2019, 58, 5049–5053. [PubMed: 30767348]

(38). Cheng Y; Clark AE; Zhou J; He T; Li Y; Borum RM; Creyer MN; Xu M; Jin Z; Zhou J; Yim W; Wu Z; Fajtová P; O'Donoghue AJ; Carlin AF; Jokerst JV ACS Nano 2022, 16, 12305–12317. [PubMed: 35878004]

(39). Xia F; Wu J; Wu X; Hu Q; Dai J; Lou X Acc. Chem. Res. 2019, 52, 3064–3074. [PubMed: 31657899]

(40). Yuan Q; Cheng Y; Lou X; Xia F Chin. J. Chem. 2019, 37, 1072–1082.

(41). Jiang T; Olson ES; Nguyen QT; Roy M; Jennings PA; Tsien RY Proc. Natl. Acad. Sci. U.S.A. 2004, 101, 17867–17872. [PubMed: 15601762]

(42). Olson ES; Jiang T; Aguilera TA; Nguyen QT; Ellies LG; Scadeng M; Tsien RY Proc. Natl. Acad. Sci. U.S.A. 2010, 107, 4311–4316. [PubMed: 20160077]

(43). Levi J; Kothapalli SR; Ma TJ; Hartman K; Khuri-Yakub BT; Gambhir SS J. Am. Chem. Soc. 2010, 132, 11264–11269. [PubMed: 20698693]

(44). Weinstain R; Savariar EN; Felsen CN; Tsien RY J. Am. Chem. Soc. 2014, 136, 874–877. [PubMed: 24377760]

(45). Chen X; Zaro JL; Shen WC Adv. Drug Delivery Rev. 2013, 65, 1357–1369.

(46). Shi H; Kwok RT; Liu J; Xing B; Tang BZ; Liu BJ Am. Chem. Soc. 2012, 134, 17972–17981.

(47). Olsen JV; Ong SE; Mann M Mol. Cell. Proteomics 2004, 3, 608–614. [PubMed: 15034119]

(48). Matsuyama S; Nao N; Shirato K; Kawase M; Saito S; Takayama I; Nagata N; Sekizuka T; Katoh H; Kato F; Sakata M; Tahara M; Kutsuna S; Ohmagari N; Kuroda M; Suzuki T; Kageyama T; Takeda M Proc. Natl. Acad. Sci. U.S.A. 2020, 117, 7001–7003. [PubMed: 32165541]

(49). TMPRSS2 RNA expression overview from the human protein atlas. Protein Atlas: https://www.proteinatlas.org/ENSG00000184012-TMPRSS2/subcellular

a

Probe name	Structure composition	Description	Calculated mass	Found mass
PyTPE	tetraphenylethene pyridinium	Dye only	533.2700 $^{1+}$	533.2697
EGTP	EEEEEEEEEGGGQAR/GG(Pra)-PyTPE	Main probe	1224.5157 $^{2+}$	1224.5128
TGP	QAR/GG(Pra)-PyTPE	Without E9	558.2945 $^{2+}$	558.2939
EGEP	EEEEEEEEEGGG**RAEG**GG(Pra)-PyTPE	No cleavage	1253.5184 $^{2+}$	1253.5164

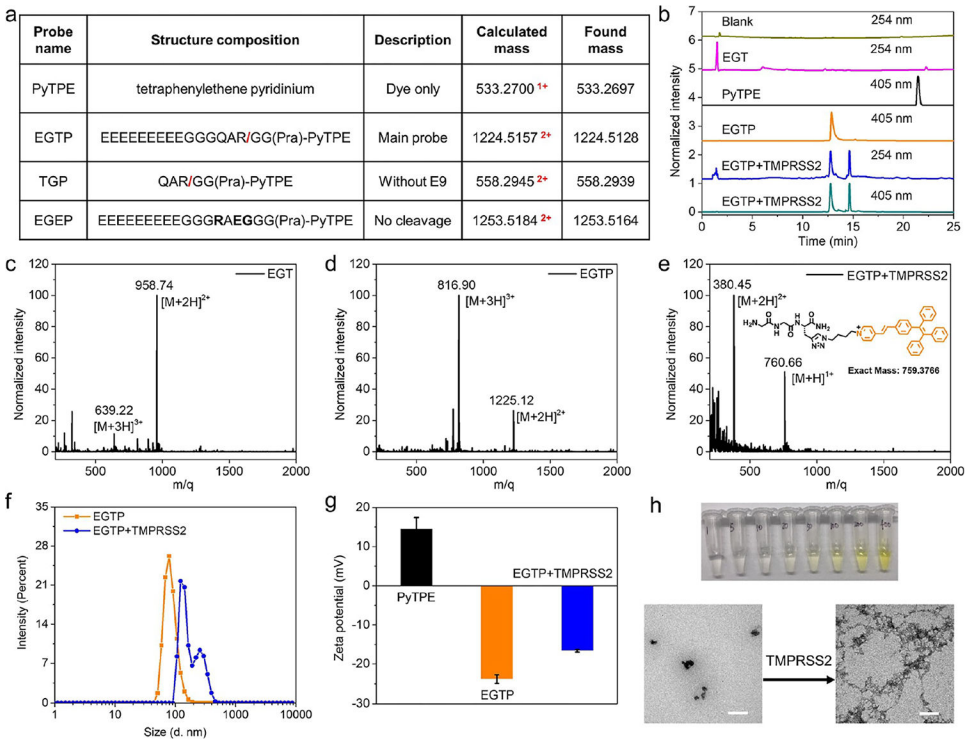

Figure 1.

Structural characterization of EGTP and its derivatives. (a) Brief description of PyTPE, EGTP, TGP, and EGEP; the red slash represents the TMPRSS2 cleavage position, the red superscript represents the number of charges in the probes. (b) High-performance liquid chromatography (HPLC) results of EGT, PyTPE, EGTP, and EGTP incubation with TMPRSS2 under 254 or 405 nm. (c–e) ESI-MS results of EGT, EGTP, and EGTP incubation with TMPRSS2. The aggregation of PyTPE after TMPRSS2 cleavage was confirmed by (f) hydrodynamic sizes via DLS, (g) ζ potential values, and (h) photographs and TEM images. In panel h, vials contained 1, 5, 10, 20, 50, 100, 200, and 400 μM EGTP solutions from left to right. Scale bars: 100 nm.

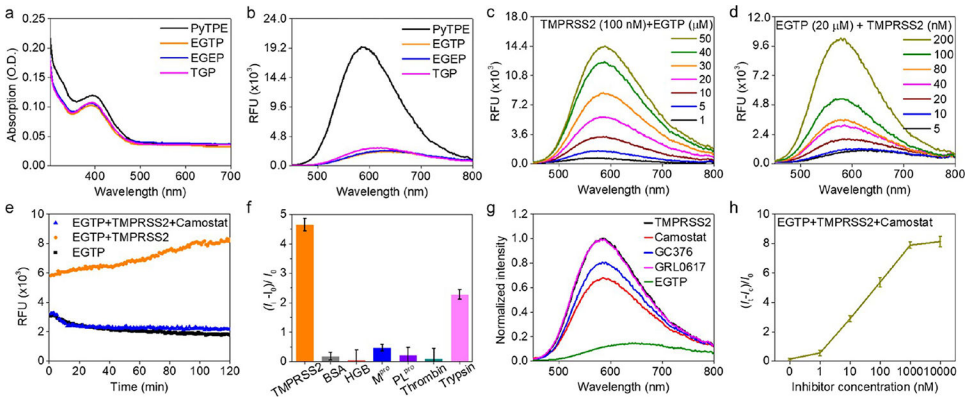

Figure 2.

Photophysical properties of EGTP and its derivatives. (a) Absorption and (b) fluorescence spectra of PyTPE, EGTP, TGP, and EGEP showed solubility enhancement with decreased fluorescence intensity after conjugation with peptides. (c,d) Fluorescence spectra and (e) kinetics of EGTP with different concentrations of TMPRSS2 and 100 nM camostat at 590 nm showed that the fluorescence increase is due to TMPRSS2. (f) Probe specificity of EGTP with 200 nM used TMPRSS2, bovine serum albumin (BSA), hemoglobin (HGB), main protease (M^{pro}), papain-like protease (PL^{pro}), thrombin (TB), and trypsin. (g,h) Impact of protease inhibitors was studied with EGTP, TMPRSS2, camostat, GC376, and GRL0617. In panel h, I_0 is the fluorescence intensity of EGTP. I_t is the fluorescence intensity of EGTP after incubation with TMPRSS2; I_c is the fluorescence intensity of EGTP after incubation with TMPRSS2 and different concentrations of camostat. Here, 20 μM of PyTPE, EGTP, TGP, and EGEP were dissolved in Tris–HCl buffer with 1% DMSO.

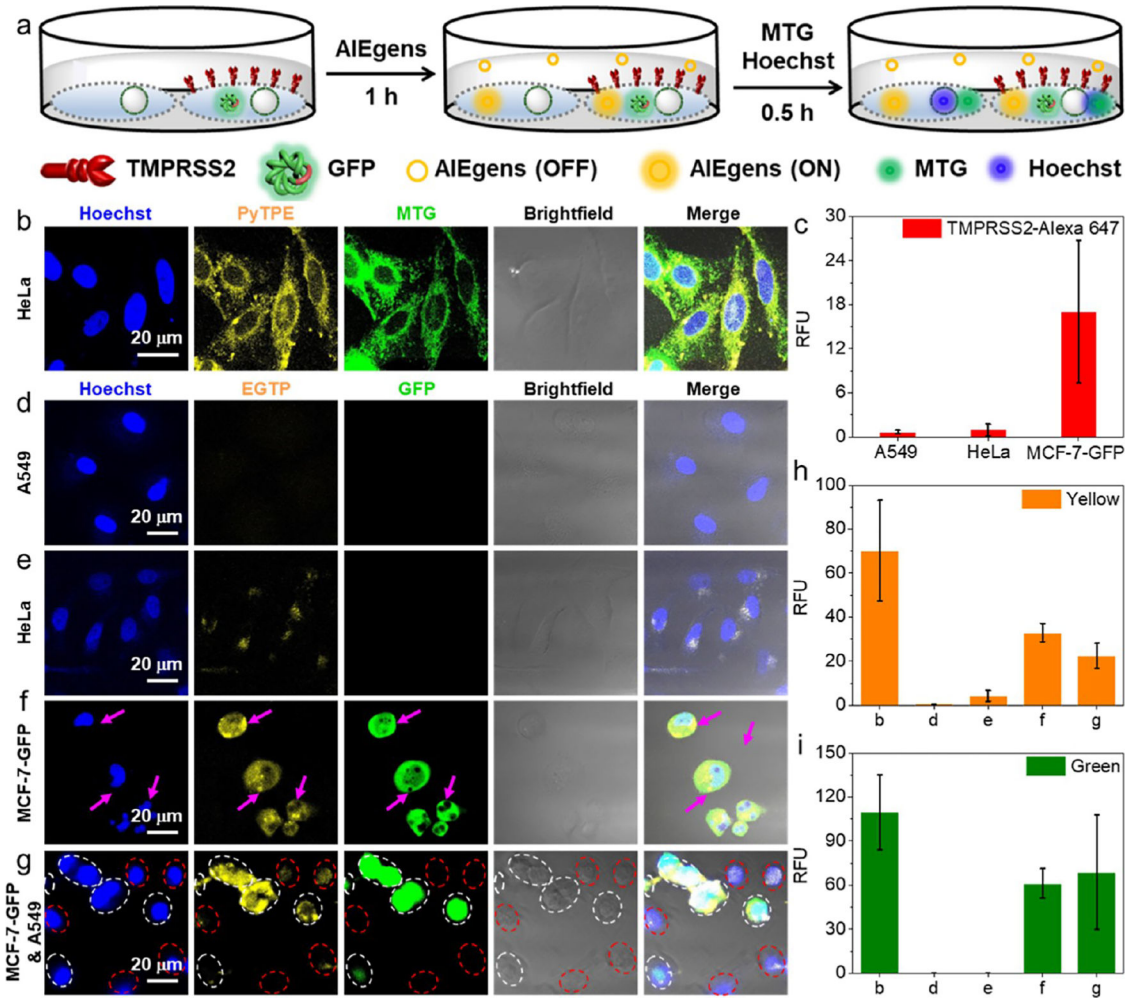

Figure 3.

TMPRSS2-selective imaging in cancer cells with EGTP. (a) The experimental scheme of TMPRSS2-selective imaging between TMPRSS2 low- and high-expressing cells during incubation with EGTP. CLSM images of (b) HeLa cells with PyTPE and MTG as well as (d) A549 cells, (e) HeLa cells, (f) MCF-7-GFP cells, and (g) MCF-7-GFP and A549 co-cultured cells with EGTP. The average fluorescence intensities of (c) A549 cells, HeLa cells, and MCF-7-GFP cells with Alexa 647-labeled TMPRSS2 antibodies, (h) yellow fluorescence representing AIEgen activation, and (i) green fluorescence representing MTG and GFP in panels (b,d–g). The MCF-7-GFP cells were activated in the green channel. The EGTP is activated in the yellow channel when cells express TMPRSS2. Pink arrows show fluorescence only from EGTP. Panel g shows white and red dotted rings denoting the MCF-7-GFP cells and A549 cells, respectively.

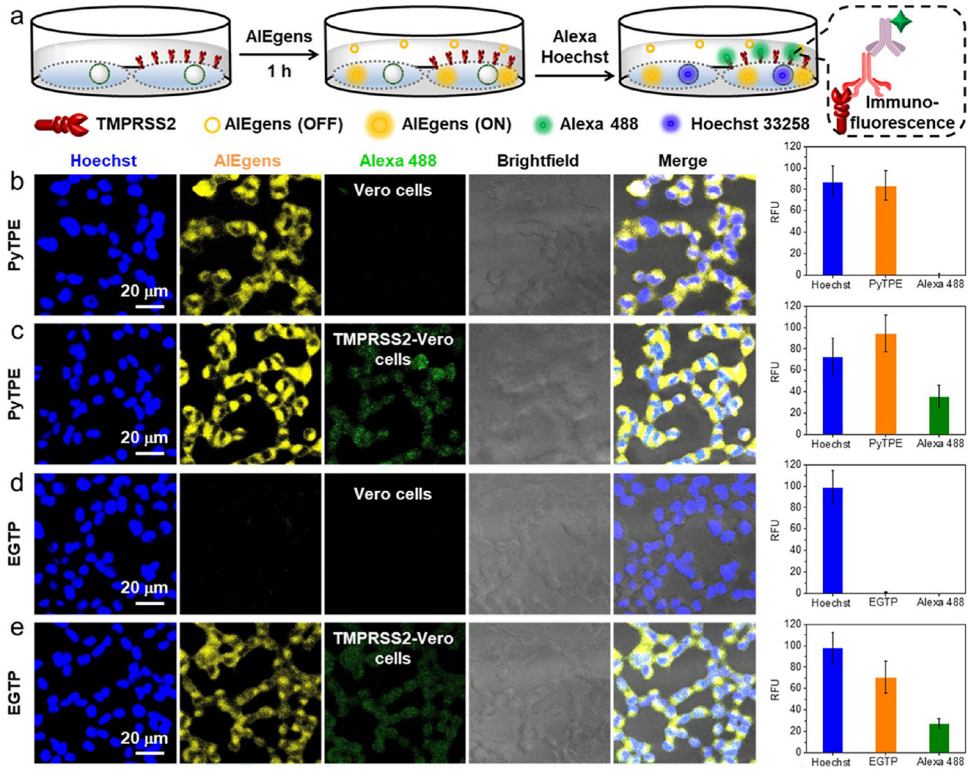

Figure 4.

Validation of EGTP in the Vero cells and TMPRSS2-Vero cells. (a) Experimental scheme of Vero and TMPRSS2-Vero cells after incubation with different AIEgens. The enlarged portion shows the mechanism of immunofluorescence imaging. CLSM images and the relative fluorescence intensities of the Vero cells with (b) PyTPE and (d) EGTP incubation and TMPRSS2-Vero cells with (c) PyTPE and (e) EGTP incubation. The EGTP and Alexa 488 are activated in the yellow and green channels when cells express TMPRSS2.

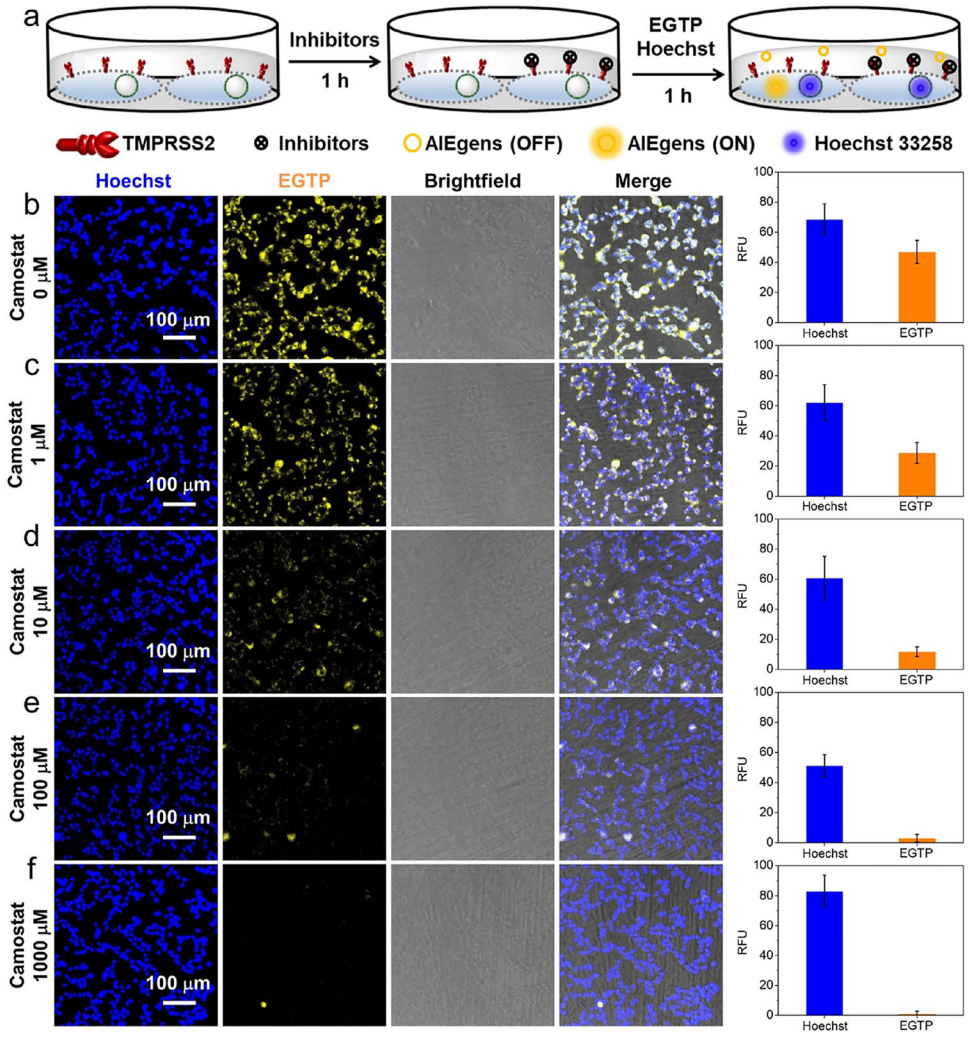

Figure 5.

Accurate TMPRSS2 inhibitor screening with EGTP and camostat. (a) Experimental scheme of TMPRSS2-Vero cells after incubation with camostat and EGTP. CLSM images and the relative fluorescence intensities of TMPRSS2-Vero cells with different concentrations of camostat and 10 μM EGTP for cell imaging. (b) 0, (c) 1, (d) 10, (e) 100, and (f) 1000 μM camostat. The EGTP is activated in the yellow channel when cells express TMPRSS2 without camostat inhibition.

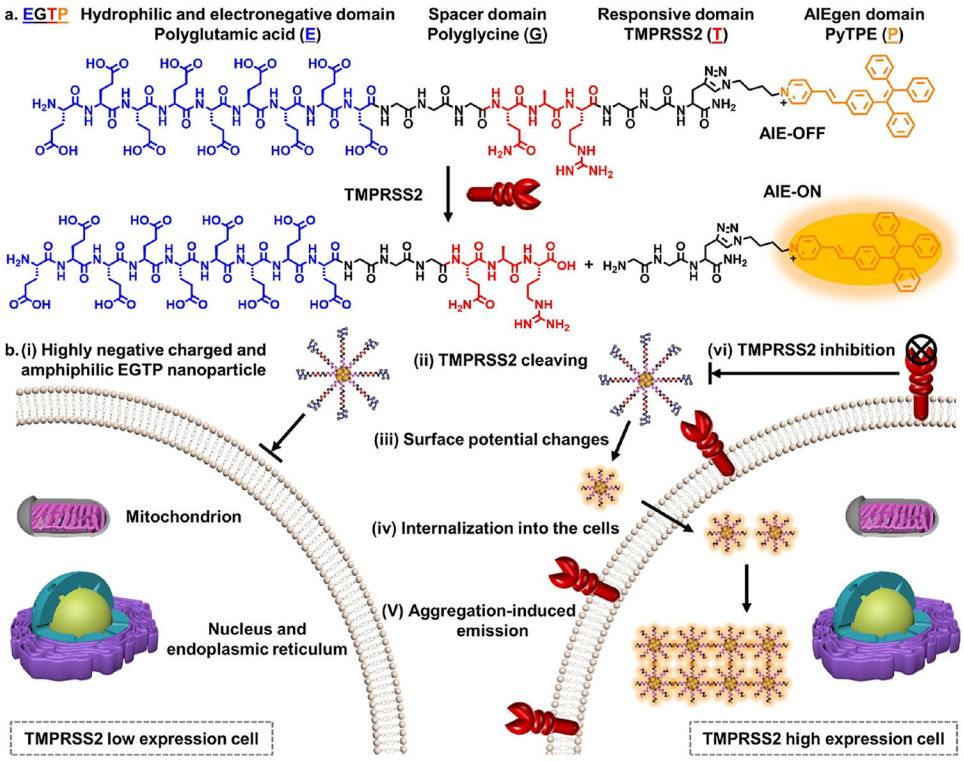

Scheme 1. Structure and Function of EGTP

; (a) Molecular Structure Changes of EGTP with TMPRSS2; (b) EGTP is Used for TMPRSS2-Responsive Imaging and Accurate Inhibitor Screening; (i) Negatively Charged Amphiphilic EGTP Cannot Cross the Cell Membrane of Cells with Low TMPRSS2 Expression; (ii) EGTP Can be Cleaved by Cells with High Expression of TMPRSS2; (iii) Surface Potential of the PyTPE Segment Changes after Removal of the Negatived Polyglutamic Acid; (iv) and Can be Internalized into the Cells; (v) High Concentrations of the PyTPE Segment Can Aggregate with Enhanced Fluorescence; (vi) No Fluorescence is Observed Once TMPRSS2 is Suppressed by Its Inhibitors.